

# Application of Transmission Electron Microscopy to Detect Changes in Pancreas Physiology

*Maša Skelin Klemen, Jurij Dolensšek, Ismael Valladolid-Acebes, Andraž Stožer and Saška Lipovšek*

## Abstract

Insulin resistance in key target organs and beta cell dysfunction due to gluco- and lipotoxicity, are the two main factors driving type 2 diabetes mellitus pathogenesis. Recently, it has been suggested that ectopic fat deposition in the pancreas, named non-alcoholic fatty pancreas disease, occurs in metabolic syndrome, and may play an etiological role in islet dysfunction and damage the exocrine pancreas, increasing its susceptibility to pancreatitis and pancreatic cancer. In this chapter, we present transmission electron microscopy (TEM) as a valuable method to detect early changes in the ultrastructure of pancreatic cells during the development of the metabolic syndrome in mice fed with a western diet (WD). Mice fed with a WD develop pathological ultrastructural alterations in the exocrine and endocrine cells. We demonstrate how to use image segmentation methods and ultrastructural morphometry to analyze and quantify structural changes in cellular organelles and evaluate the presence of lipid droplets, autophagic structures, and vacuolization. Since ultrastructural lesions can be detected early during the progression of the metabolic syndrome, are in many aspects subtle, and by far precede cell apoptosis, necrosis, fat infiltration, and overt functional changes, TEM is not only a suitable but probably the crucial method for detecting early pancreas dysfunction.

**Keywords:** pancreas physiology, exocrine cells, endocrine cells, ultrastructure, metabolic syndrome, type 2 diabetes mellitus, western diet

## 1. Introduction

The number of people with type 2 diabetes mellitus (T2DM) is growing rapidly worldwide and has already exceeded 530 million in 2021 [1]. Because of the severe consequences of T2DM for patients and the enormous burden on the healthcare system, a lot of research is focused on understanding the development of T2DM. The healthy pancreatic beta cells secrete insulin at a basal rate throughout the day and increase secretion in response to stimulation with nutrients, especially glucose, and other neurohormonal secretagogues, such as acetylcholine and GLP-1, after a meal [2–4]. Understanding the pathophysiology of early phases of glucose tolerance

disruption associated with morphological and functional beta cell changes present in insulin-resistant people susceptible to the development of T2DM is especially important and has been the focus of many research groups [5–9]. However, to date very limited information is available about the ultrastructural alterations of beta cells during the early stages of T2DM development [10–13].

Thus, the aim of our chapter is to present the importance and illustrate the usefulness of transmission electron microscopy (TEM) in the research field of pancreas physiology through specific and easily reproducible examples. TEM is a technique used to obtain ultrahigh-resolution images of different samples. The prototype of the transmission electron microscope was developed by Ernst Ruska and Max Knoll in 1931. Since then, TEM has been extensively used in biomedical research, helping us deepen our knowledge about the ultrastructure of cells and understanding the cellular processes. TEM was first used to identify specific features of pancreatic endocrine and exocrine cells in the mid-1950s by Paul Lacy [14] and George Palade [15], respectively. TEM exploits the wavelength properties of electrons to provide greater spatial resolution than the resolution achieved using photons in light microscopy (LM). In TEM, a beam of high-voltage electrons is emitted by the electron gun and then passed through the sample. The most challenging part of TEM is the preparation of samples that are thin and robust enough to allow electrons to penetrate the sample on the one hand and survive the damage caused by the electron beam on the other. In this chapter, TEM is implemented as an appropriate research method that allows us to detect very subtle structural changes in pancreas cells of mice fed with a western diet (WD). Here, we focus on sample preparation, microscopy, and quantitative analysis of ultrastructure, together with some representative results, to illustrate the utility and emphasize the importance of TEM in pancreas research. A comprehensive analysis of ultrastructural changes in WD-fed mice with partly compensated diabetes mellitus will be present in detail elsewhere.

In the first part of this chapter, we briefly summarize the basic anatomical features of the pancreas in humans and mice and describe the main physiological characteristics of the endocrine and exocrine pancreas. Next, we describe the development of T2DM, focusing on the role of obesity and key pathophysiological events. In the central part of this chapter, we discuss the ultrastructural morphology and describe the methodology used for ultrastructural morphometry of the exocrine and endocrine pancreas during the early stages of WD-induced T2DM development.

## **2. Structure and function of the pancreas**

The pancreas is an unpaired gland of the alimentary tract with two different but complementary functions: the production of digestive enzymes and alkaline fluid in exocrine cells that help with the breakdown of energy-rich nutrients and the synthesis by endocrine cells of hormones needed to control the storage and usage of energy-rich nutrients [16]. In humans, the pancreas is a well-defined organ with three major parts: the head, the body, and the tail, extending from the duodenum to the spleen [17, 18]. In mice, the pancreas is not as well-defined as in humans but is rather diffusely distributed in a dendritic manner while it is still composed of three major parts: the duodenal lobe, the largest splenic lobe, and the smallest gastric lobe [19]. A fibrous capsule surrounds the pancreas, and the connective tissue extending into the gland divides the parenchyma into larger lobes and smaller lobules [18, 20]. Each lobule is composed of acini that consists of pyramid-shaped acinar cells [21]. The exocrine part accounts for

96–99% and the endocrine islets of Langerhans for the remaining 1–4% of total pancreas parenchyma [22, 23]. In mice, the islets are mainly interlobular, while in humans they are usually intralobular, mostly on the edge of lobules [24, 25]. Despite some differences [26], islets of Langerhans from mice and men possess many structural and functional similarities [27, 28]. They are round to oval, vary in size, and range from a few to several thousand endocrine cells. Importantly, the islet size distributions are similar in humans and mice (and also many other species) [22]. At least five different types of endocrine cells can be found in islets in both species [27]. Most numerous are the beta cells that synthesize and secrete insulin. Alpha cells secrete glucagon, while delta cells and PP cells release somatostatin and pancreatic polypeptide, respectively. Finally, epsilon cells are the least abundant, synthesizing and secreting ghrelin [23–25].

As mentioned above, the exocrine pancreas plays a crucial role in the enzymatic digestion of carbohydrates, proteins, and lipids and secretes a bicarbonate-rich fluid [29–31]. The enzymes are stored in an inactive proenzyme form in the so-called zymogene granules located at the apical membrane of acinar cells and are released in response to stimulation by neurohormonal secretagogues, such as acetylcholine and cholecystokinin, via exocytosis. The fusion of granules with the apical plasma membrane releases the enzymes first into the acinar lumen, from where they pass via the ductal tree into the small intestine [32]. In contrast, islets release their hormones into the numerous islet blood capillaries that drain into the portal venous system. In the liver and other key target tissues, such as the skeletal muscle and adipose tissue, insulin acts as a key anabolic hormone, promoting glycogenesis, glycolysis, lipogenesis, and proteinogenesis, and suppressing gluconeogenesis, lipolysis, and proteolysis [33–35]. On the other hand, glucagon acts mainly in the liver, where it promotes glycogenolysis and gluconeogenesis, and inhibits glycolysis and glycogenesis [36, 37].

### **3. The role of obesity in the development of type 2 diabetes**

The decrease in insulin action indicates insulin resistance, the main hallmark of T2DM [38]. Several factors play a role in the development of insulin resistance, with obesity probably being the most important one [39]. During the last three decades, obesity has reached an epidemic stage in all age groups [40]. Increased intake of energy-dense foods containing a high percentage of fat and carbohydrates, combined with a lack of physical activity, leads to a net positive energy balance and represents the primary cause of obesity. The first stages of obesity are hypertrophy and hyperplasia, where adipocytes try to meet the demand to store excessive energy. When levels of free fatty acids and triglycerides exceed the metabolic capacity of adipose tissue, they accumulate as ectopic fat in non-adipose tissue such as the liver, pancreas, skeletal muscles, and heart [41]. The regional distribution of adipose tissue is particularly important for the development of disorders of glucose and lipid metabolism [42, 43]. The fat infiltration in the liver and pancreas in the absence of excess alcohol intake is termed non-alcoholic fatty liver disease (NAFLD) and non-alcoholic fatty pancreas disease (NAFPD), respectively [44]. Due to fat accumulation in hepatocytes, NAFLD leads to inflammation, fibrosis, cirrhosis, and liver cancer and critically affects insulin sensitivity in the liver [44–46]. NAFPD plays a similar role in the dysfunction of the endocrine and exocrine pancreas leading to exacerbation of acute pancreatitis and increasing the susceptibility to pancreatic cancer [46–50]. Although the concept of the NAFPD was introduced only a few years ago [51], the correlation between fat infiltration and pancreas was first described almost a century ago on

obese cadavers having larger pancreata compared to non-obese cadavers [52, 53]. Importantly, over the last decade, it has been demonstrated convincingly that most of the morphological, functional, and clinical features of T2DM are reversible with sufficient weight loss and that these positive changes depend on the level of hepatic and pancreatic fat reduction [54–56].

Although insulin resistance is one of the main features of T2DM, it is not sufficient for the development of T2DM. Despite increasing insulin resistance, present long before the onset of diabetes, individuals with preserved beta cell capacity can stay normoglycemic for several years due to compensatory insulin hypersecretion. Furthermore, a certain proportion of individuals with insulin resistance never develop T2DM. The idea has been put forward that there may be a personal fat threshold or an individual level of susceptibility to developing T2DM at a given body mass index, with the main mechanisms behind this attractive hypothesis being varying degrees of fat accumulation in the liver and the pancreas, together with varying individual responses to this accumulation [57]. An obese subject with insulin resistance can secrete 2–5 times more insulin compared to lean non-diabetic individuals in response to a glycemic load, but when the adaptive capacity of the beta cells fails, T2DM occurs [58]. Several studies have shown that the first phase of insulin secretion is primarily affected, resulting in impaired glucose tolerance. During the progression of T2DM, the second phase of insulin secretion is further lost. Post-translational defects in insulin synthesis also occur, resulting in increased proinsulin secretion, and by the time the diagnosis of T2DM is made, the beta cell function is already typically reduced by 80% [59]. This beta cell failure is responsible for transitioning from an insulin-resistant compensated state to overt T2DM and remains to be elucidated in details. It probably involves an initially inadequate beta cell mass and an insufficiently increased response of the existing beta cells to increased insulin demand [60]. Noteworthy, the susceptibility of beta cells themselves to developing insulin resistance may play an important pathophysiological role [61]. Individuals with T2DM can display changes in beta cell mass, either due to a decrease in beta cell proliferation or/and an increase in cell apoptosis [62]. In T2DM patients, the apoptosis rate is increased severalfold compared to normoglycemic individuals [63], a phenomenon confirmed by ultrastructural analysis using TEM [64]. Furthermore, during T2DM gradual dedifferentiation of beta cells occurs in animal models, while the role of dedifferentiation during the development of human T2DM is controversial and less well-studied [63, 65–68]. Chronic exposure of islets to elevated levels of glucose, fatty acids, and amino acids results in ER stress due to increased insulin synthesis and secretion [69]. The protein folding capacity of ER becomes exceeded, which leads to the activation of the so-called unfolded protein response (UPR) and consequently to the inhibition of protein translation [70, 71]. Gluco- and lipotoxicity cause a vicious cycle of continuous deterioration of the glucometabolic state and eventually impair insulin secretion and increase apoptosis. In T2DM, not only the islet cells are affected, but also the pancreatic acinar cell viability and growth decrease, leading to increased apoptosis and replacement by fat [72, 73]. Importantly, intracellular fat in acinar cells may affect beta cell function in a paracrine manner through the release of adipokines. It is also likely to play a role in pancreatic carcinogenesis, seems to be associated with changes in innervation, and may initiate an acinar-to-adipocyte trans-differentiation [56].

#### **4. Application of TEM in pancreas physiology**

Glucose-induced insulin secretion is based on oxidative metabolism, thus mitochondrial function is of crucial importance for beta cells [74]. Mutations in mitochondrial

DNA result in reduced insulin secretion and hyperglycemia [75]. The genetic background is not the only factor affecting mitochondrial function. The diabetic environment, with chronic hyperglycemia, can also affect mitochondria [76]. Such a milieu could be responsible for the progression of T2DM and the reduced capacity of insulin release in these patients. Mitochondria appear round-shaped and hypertrophic in endocrine cells from T2DM islets [76–78]. Besides mitochondria, the structure of other cellular organelles is also altered [79]. The volume density of the endoplasmic reticulum is typically increased, and autophagic vacuoles are present [78, 80, 81]. TEM is also a very useful technique that enables us to identify apoptotic cells [82].

Several studies showed that TEM is suitable to detect morphological characteristics of the diabetic pancreas, but only a few studies have reported results in quantitative terms. Due to the large variability and plasticity of cells and their organelles, especially mitochondria, qualitative evaluations are not sufficient [83]. Furthermore, quantitative morphometry is needed to evaluate subtle structural changes early during the progression of the metabolic syndrome that may precede overt functional changes occurring during the development of T2DM.

Since mouse models of T2DM exhibit comparable developmental features and can provide significant insight into the mechanisms of T2DM development in humans [84], they are widely used in these studies. From several animal models, C57Bl/6 J mice have been the most susceptible to the development of the metabolic syndrome and diet-induced diabetes [85–89]. We performed the morphological and morphometric evaluation of pancreatic endocrine and exocrine tissue obtained from C57Bl/6J mice fed with control diet (CD) or western diet (WD). During 8 weeks on WD, these mice developed obesity, hyperglycemia, and hyperinsulinemia (data not shown). Pancreatic tissue samples were taken in parallel with the preparation of acute pancreas tissue slices intended for electrophysiological studies, confocal calcium imaging, and expression analyses. Although the functional response to glucose in terms of intracellular calcium concentration changes and sensitivity of the exocytotic machinery to calcium were well preserved in WD mice (data not shown), TEM revealed severe morphological changes in the endocrine and exocrine part of the pancreas. In the following section, we demonstrate how to use image segmentation methods and ultrastructural morphometry to analyze and quantify structural changes in the rough endoplasmic reticulum, mitochondria, and exocytotic vesicles and vacuolization in the endocrine and exocrine part of the pancreas from control animals and animals fed with WD. These ultrastructural lesions presented below can be detected early during the progression of the metabolic syndrome and precede cell apoptosis, necrosis, fat infiltration, and overt functional changes. Therefore, TEM enables a more direct assessment of the functional characteristics of the pancreatic tissue and is therefore a suitable and probably the crucial method for detecting alterations associated with early pancreas dysfunction.

## **5. Sample preparation and analysis**

### **5.1 Ethical statement**

The study protocol was approved by the Administration for Food Safety, Veterinary Sector and Plant Protection, Ministry of agriculture, Forestry and Food Republic of Slovenia (approval number: U34401–12/2015/3). The study was conducted in strict accordance with all national and European recommendations pertaining to care and work with laboratory animals, and every effort was made to minimize animal suffering.

## 5.2 Animals, tissue preparation, light, and transmission electron microscopy

Experiments were performed on 20–22-week-old male C57BL/6 J (RRID: IMSR\_JAX:000664) mice purchased from Charles River (**Figure 1A**). Upon weaning, mice were fed with a standard rodent diet (CD, R70, Lantmännen, Stockholm, Sweden) with 72% of kcal from carbohydrates, 10% from fat, and 18% from protein until 12 weeks of age. From 12 to 20 weeks of age, a control group continued to be fed with CD while the second group was fed with WD (D12079B, Research diets inc., New Jersey, USA) containing 43% kcal from carbohydrates, 40% from fats and 17% from proteins (**Figure 1B**). Water was available *ad libitum*. Mice were housed in individually ventilated cages (Allentown LLC, USA) in groups of 1–4 animals per cage at 20–24°C, 45–65% relative humidity, and a 12-hour day-night lighting cycle. The bright part of the cycle was between 7 pm and 7 am. Mice were weighed before sacrifice.

Acute pancreas tissue slices from CD and WD mice were prepared as described previously [90–92]. For light microscopy (LM) and transmission electron microscopy (TEM), a small piece of the pancreatic splenic lobe was clamped using hemostatic forceps to avoid the leakage of agarose into this part of the pancreas. After removal from the body, small fragments of the pancreas were fixed in 2.45% glutaraldehyde and 2.45% paraformaldehyde in a 0.1M sodium cacodylate buffer (pH 7.4) at room temperature for 3 h, and at 4°C for 12 h. The tissue was washed in a 0.1 M sodium cacodylate buffer (pH 7.4) at room temperature for 4 h and post-fixed with 2% OsO<sub>4</sub> at room temperature for 2 h. After washing in a 0.1 M sodium cacodylate buffer (pH 7.4) at room temperature for 3 hours, the tissue was dehydrated in a graded series of ethanol (50%, 70%, 90%, 96%, and 100%, each for 30 minutes at room temperature). The pieces of the tissue were embedded in TAAB embedding resin (Agar Scientific Ltd., Essex, England). For LM, semithin sections (2 μm) were stained with 0.5% toluidine blue in an aqueous solution. For TEM, ultrathin sections (70–75 nm) of the tissue were stained with uranyl acetate and lead citrate and analyzed with a Zeiss EM 902 transmission electron microscope.

## 5.3 Structure of the exocrine and endocrine pancreas

### 5.3.1 Qualitative analysis of exocrine and endocrine cell ultrastructure

The pancreas is composed of exocrine and endocrine tissue and this functional specialization can readily be recognized microscopically (**Figure 2**).

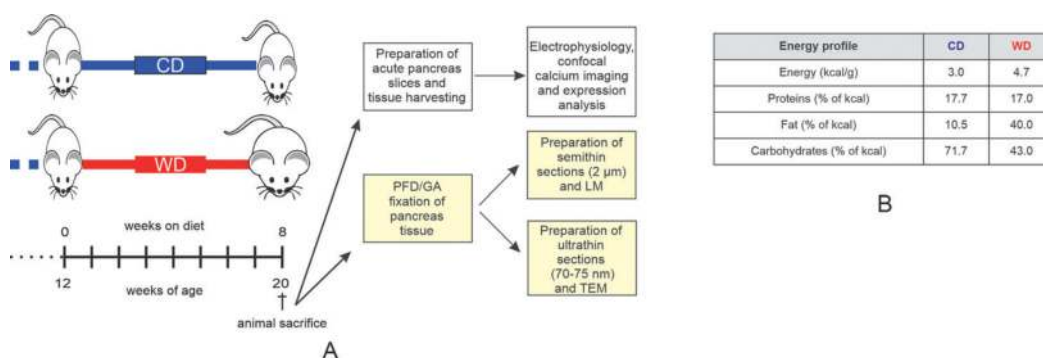


**Figure 1.** Study design (A) timeline of the study. The part of the project shown in yellow is presented in this chapter. (B) Energy profile of control diet (CD) and western diet (WD).

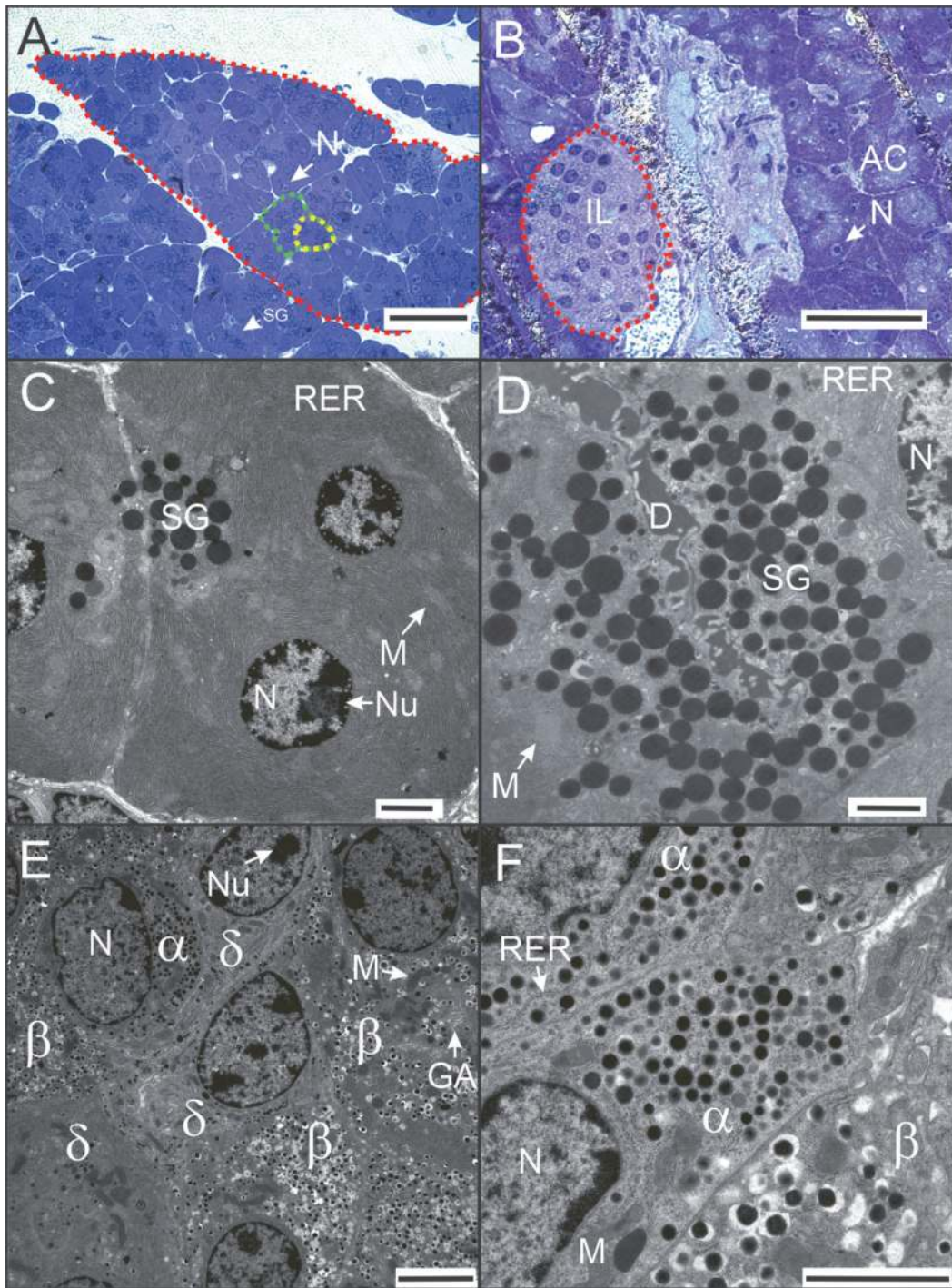


**Figure 2.** Mice are fed with control diet (CD). (A) and (B) Semithin sections of the pancreas. (A) Exocrine part of the pancreas is composed of acinar cells (one cell marked by the yellow dotted line), organized in acini (one acinus marked by the green dotted line) and lobules (one lobule marked by the red dotted line). (B) Endocrine cells forming a Langerhans islet are seen as brighter stained cells (red dotted line). (C–F) Ultrathin sections of the pancreas. (C) Exocrine cells are easily recognized by their large size, typical shape, by abundant rough endoplasmic reticulum, and secretory granules. (D) The majority of secretory granules are found in the apical part of the cell. (E) and (F) endocrine cells can be distinguished by the fine structure and size of their secretory granules. In all endocrine cells, well-developed rough endoplasmic reticulum, Golgi apparatus, and numerous mitochondria are seen. AC, acinar cell;  $\alpha$ , alpha cell;  $\beta$ , beta cell;  $\delta$ , delta cell; D, duct; IL, islet of Langerhans; GA, Golgi apparatus; M, mitochondrion; N, nucleus; nu, nucleolus; RER, rough endoplasmic reticulum; SG, secretory granules. Scale bars: (A) and (B) 50  $\mu\text{m}$ ; (C) 2.5  $\mu\text{m}$ ; (D) 2  $\mu\text{m}$ ; (E) 5  $\mu\text{m}$ ; (F) 2.5  $\mu\text{m}$ .

### 5.3.1.1 Normal exocrine and endocrine cell ultrastructure

The majority of tissue consists of pyramid-shaped exocrine cells (**Figure 2A–C**). These cells form clusters or acini around small ducts and are organized in lobes with thin fibrous tissue. The exocrine cells produce inactive digestive enzymes, seen in the cytoplasm packed in secretory vesicles (**Figure 2C and D**), and secrete them into the intercalated ducts which they surround (**Figure 2D**). In each acinus, the exocrine cells are located around the intercalated ducts, with their narrow apical parts oriented to the duct (**Figure 2C and D**). The exocrine cells have a round or oval nucleus (**Figure 2C**), located basally. The most prominent structure of the exocrine cells is the rough endoplasmic reticulum (**Figure 2C**) which is present in all different parts of the cell. Numerous round electron-dense secretory vesicles are seen in the perinuclear and apical cytoplasm (**Figure 2C and D**). The oval mitochondria (**Figure 2C and D**) are found in different parts of the cell.

The endocrine cells are distributed throughout the pancreas (**Figure 2B**) as interlobular positioned clusters of cells termed islets of Langerhans. In the islets of Langerhans (**Figure 2B**) alpha, beta and delta cells can be distinguished (**Figure 2E and F**). They are characterized by numerous secretory vesicles. Glucagon granules of alpha cells are large dense-core vesicles and some of them have a pale halo. The core of the granule is of a similar diameter to insulin granules, but the whole granule is smaller by at least 50% (200 nm vs. 350 nm). Insulin-containing vesicles in beta cells are the largest with large clear peripheral halos. Somatostatin-containing granules of delta cells in mice are the smallest and lozenge-shaped (**Figure 2E and F**) [93–96]. In the cytoplasm of all types of endocrine cells, abundant rough endoplasmic reticulum, Golgi apparatus, and many oval mitochondria are present (**Figure 2E and F**) [97].

### 5.3.1.2 Ultrastructural changes in WD mice

Comparing the ultrastructure of pancreatic cells in control mice (CD; **Figure 2**) and mice fed the western diet (WD; **Figures 3A and B, 4B, 5E, 7E, and 8D**), we observed many important differences. In the exocrine pancreas of WD mice many necrotic cells (**Figures 3A and 4B**) are present. In some acinar cells, lipid droplets are seen in the

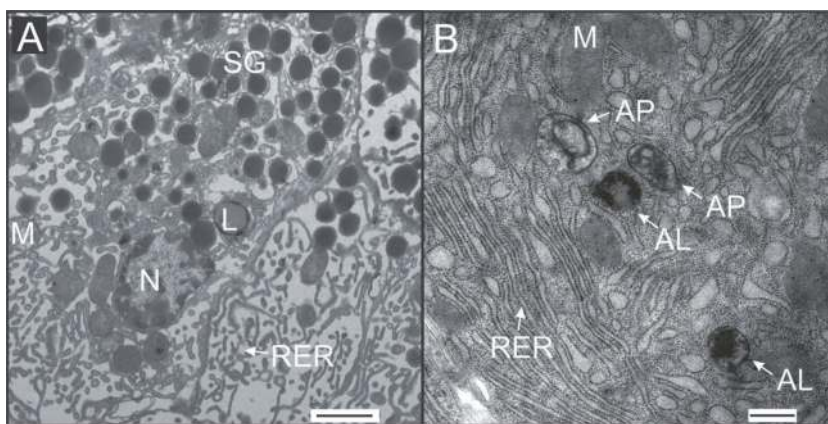


**Figure 3.** Mice are fed with western diet (WD). (A) and (B) Ultrathin sections of the pancreas. (A) A necrotic acinar cell containing a lipid droplet in the cytoplasm. (B) Autophagosomes and autolysosomes in the cytoplasm of an acinar cell. AL, autolysosome; AP, autophagosome; L, lipid droplet; M, mitochondrion; N, nucleus; SG, secretory granules; RER, rough endoplasmic reticulum. Scale bars: (A) 2  $\mu$ m; (B) 500 nm.



cytoplasm (**Figure 3A**). In many cells, numerous autophagic structures, i.e., autophagosomes, autolysosomes (**Figure 3B**), and residual bodies are found. The mitochondria (**Figure 4B**) and rough endoplasmic reticulum (**Figure 5E**) seem to be disorganized, therefore these structures were analyzed in detail.

The structure of the islets of Langerhans in mice fed by WD is non-compact, inhomogeneous, containing more extracellular spaces than in mice fed by CD. There are many necrotic cells in different parts of the islets. In the cytoplasm of endocrine cells, some lipid droplets and many autophagic structures, i.e., autophagosomes, autolysosomes, and residual bodies can be found. Structural differences are also seen in the mitochondria and rough endoplasmic reticulum.

### 5.3.2 Quantitative analysis of selected cellular structures

Structural characteristics of mitochondria, rough endoplasmic reticulum, zymogen granules, and vacuoles were studied. To accurately analyze various cell compounds, it is necessary to select TEM images taken at the same magnification.

#### 5.3.2.1 Analysis of mitochondria

Since mitochondria are crucial for normal beta cell stimulus-secretion coupling and their ultrastructure is altered during the development of T2DM, we analyzed them in more detail. First, we outlined all the mitochondria in the visual field and calculated the surface area in  $\text{nm}^2$ . To quantitatively assess the condition of mitochondria, we measured the following shape descriptors: circularity, roundness, aspect ratio of the best fit ellipse, and solidity using Fiji software (NIH) [98].

Circularity (C) is a shape parameter that can mathematically indicate the degree of similarity to a perfect circle. A value of 1.0 indicates a perfect circle. When the circularity value approaches 0.0, the shape becomes less and less circular. Circularity is defined by the equation

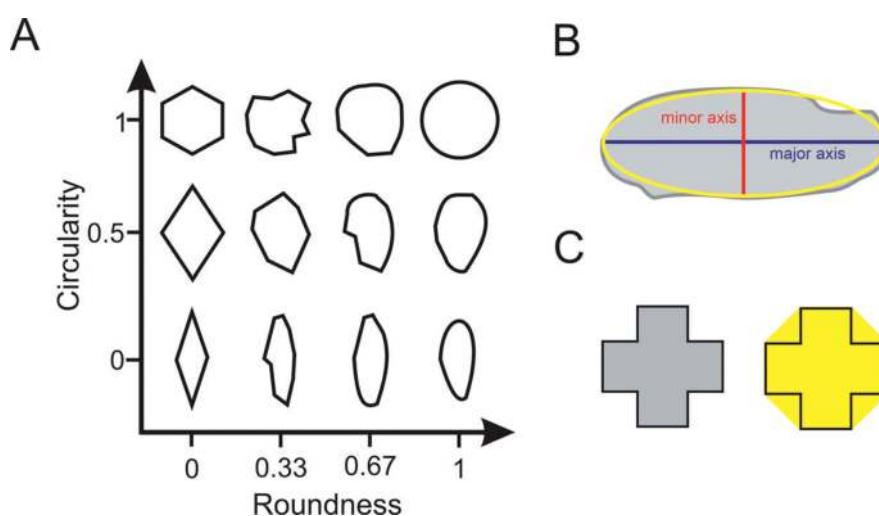


**Figure 4.** Shape descriptors. (A) Circularity versus roundness. (B) Sketch of a mitochondrion (gray) with an overlay of the best fit ellipse (yellow), the major axis of the best fit ellipse (blue), and the minor axis of the best fit ellipse (red). The major axis is used in determining roundness (Eq. (2)) and aspect ratio (Eq. (3)). (C), the shape area (gray, left) and the convex hull area (yellow, right) are used to determine the solidity.

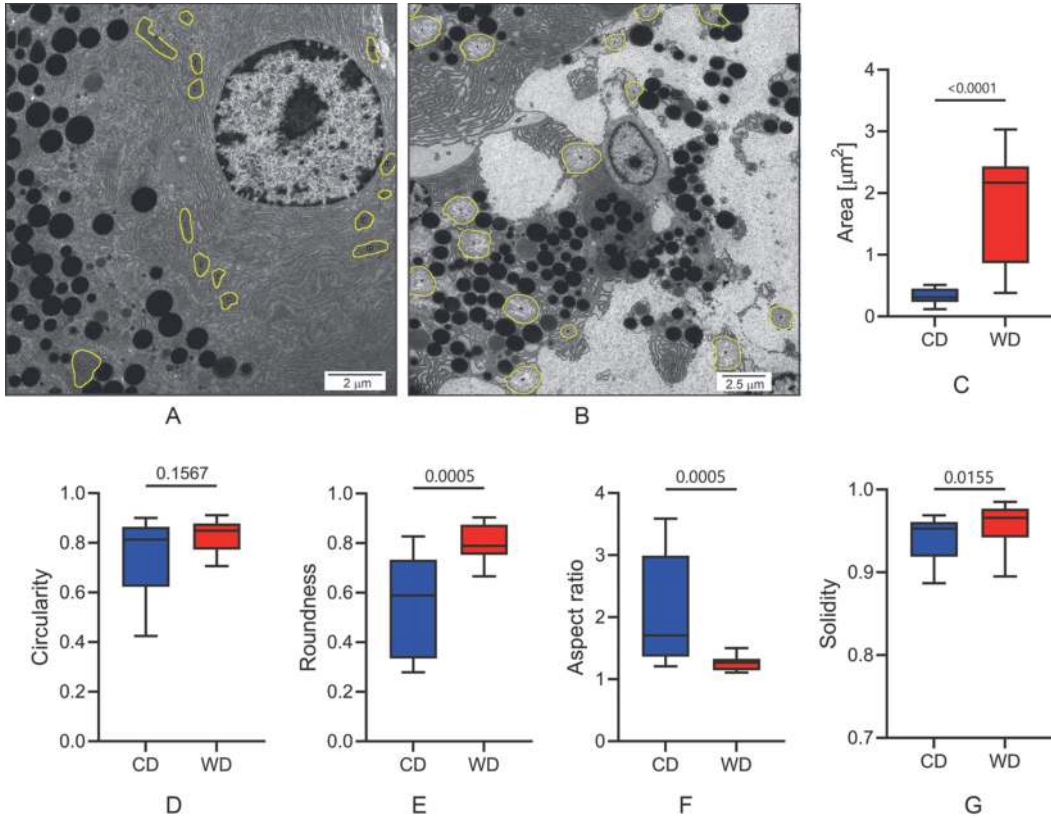


**Figure 5.** Analysis of the mitochondria from a CD and a WD mouse. Labeled mitochondria in the image of the exocrine pancreas from the (A) CD and (B) WD mouse. Analysis of the (C) surface area, (D) circularity, (E) roundness, (F) aspect ratio and (G) solidity of an image from CD and WD mouse. Data were pooled from the following number of ROIs from the CD/WD image: 14/16. Data were analyzed using the Mann–Whitney U test, *p* values are indicated on graphs.

$$C = 4\pi \frac{Area}{Perimeter^2} \quad (1)$$

Roundness (R) on the other hand, characterized by

$$R = \frac{4Area}{\pi \text{ major axis}^2} \quad (2)$$

is similar to circularity, but it is insensitive to irregular borders along the perimeter of the mitochondria and takes into account the major axis of the best fit ellipse. For an illustrative explanation of the differences between circularity and roundness, see **Figure 6A**.

From the best fit ellipse fit to each mitochondrion, the major and minor axes were determined, and the aspect ratio (AR) was calculated by the following equation:

$$AR = \frac{\text{major axis}}{\text{minor axis}} \quad (3)$$

AR measures the ratio of an object's height to its width (**Figure 6B**). Therefore, the aspect ratio is equal to one for a perfect circle and increases with an increase in deformation.

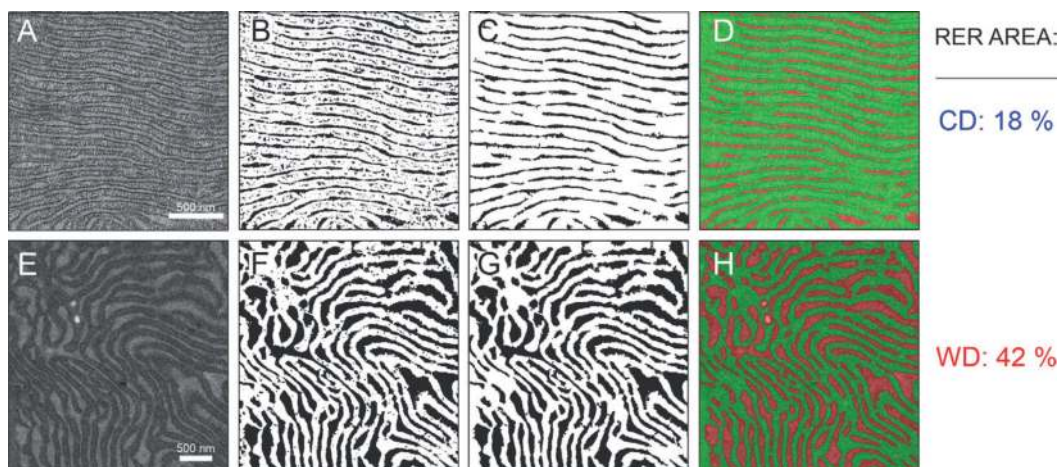


**Figure 6.** Quantitative analysis of the RER. Representative TEM images from a CD (A) and a WD (E) mouse. The quantification pipeline involves segmentation (B and F), a binary mask depicting RER cisternae in black and cytosol in white), followed by RER determination using particle analysis on the segmented image (C and G). Overlay of the binary masks on the TEM images (D and H), RER cisternae in red, and cytosol in green). Exemplary percentages of the area covered by the RER cisternae are shown in the top right (CD mouse) and bottom right (WD mouse).

At the end, solidity (S) was measured using the same Fiji software. Solidity describes the extent to which shape is convex or concave. Taking the area within the mitochondrion and dividing it by the area enclosed by a convex hull provides information about the solidity of the shape (**Figure 6C**). Solidity of a perfectly convex structure is 1, but when the structure becomes more concave, the solidity will deviate from 1. The solidity is defined by

$$S = \frac{\text{area}}{\text{convex area}} \quad (4)$$

In the bullet points that follow, we describe each analysis step in detail.

1. Open an image in Fiji.
2. Select the straight line tool from the navigation pane and draw a straight line across the scale bar. The straight line must be precisely the same length as the scale bar.
3. In the “Analyze” menu, select “Set Scale”. When the set scale dialog box opens, enter the value of a scale bar into the “Knowing Distance” box, and in the “Unit of length” box, determine the unit of the scale bar from the image. Click the “OK” button. Now you have set the scale for this particular image.
4. Use the “freehand selection” tool from the toolbar and encircle the first mitochondrion on the image. After the right mouse click within the selected encircled mitochondrion, choose “Add to ROI Manager” from the dialog box.
5. Now encircle the next mitochondrion and click “Add” in the ROI Manager. In the same way, encircle all the mitochondria in the image.
6. In the “Analyze” menu, select “Set measurements” and tick the desired parameters from the dialog box. For the analysis of mitochondria, we selected “Area” and “Shape descriptors”. Click the “OK” button.

7. Now everything is set to analyze all the mitochondria from the image. Select “Measure” in the “Analyze” menu, and a new window with results will pop out. Save the results by selecting “Save as” from the “File” menu of the “Results” window.
8. Now you can analyze the new image in the same way. Remember that the scale must be set again when analyzing the next image.

In **Figure 4** one can observe the results of the above analysis on mitochondria of two representative images of the exocrine pancreas from a CD (**Figure 4A**) and a WD (**Figure 4B**) mouse.

#### 5.3.2.2 Analysis of rough endoplasmic reticulum (RER)

Quantitative analysis of the surface area covered by the RER cisternae on TEM images can provide valuable insight into functional changes in both acinar and endocrine cells. Quantification of the TEM data, in general, involves manual annotation of structures of interest. This approach proved to be an extremely time-consuming process for quantification of the RER data, as the organelle forms a complex and interconnected network of cisternae. To overcome this issue, Trainable Weka Segmentation (TWS, available as Fiji/ImageJ plugin) provides a machine learning tool capable of automated segmentation [99]. A limited number of manual annotations on a sample (training) TEM image produces a classifier that can be applied to the remaining data to segment images automatically. The following pipeline describes steps for RER analysis:

1. Image segmentation: TWS produces a segmented image that reliably separates RER cisternae from the cytosol (**Figure 5B** and **F**, compare with **Figure 5A** and **E**, respectively).
2. Particle analysis: subsequent particle analysis on the segmented image excludes unwanted objects based on the size exclusion criterion that removes small objects that were detected mostly within RER cisternae (**Figure 5C** and **G**). If needed, manually delete unwanted objects.
3. Quantification of data: the resulting binary mask improves partitioning compared to TWS segmentation alone (**Figure 5D** and **H**). The resulting image segments allow for quantification of RER abundance, expressed as the relative area covered by RER cisternae (% RER area). This approach detected a large increase in % RER area in WD mice compared with CD mice in the given cell (42% vs. 18%) (**Figure 5**).

#### 5.3.2.3 Analysis of zymogen granules

Zymogen granules form a reserve pool of digestive enzymes that are secreted from acinar cells after stimulation. The granules are well visible on TEM images and detecting a change in a number of granules per cell, cumulative granule area per cell, or granule size could suggest a functional change in their physiology. Manual counting of granules is the simplest method to quantify zymogen content; however, it relies on an assumption of typical granule size, and it is a relatively time-consuming approach. Alternatively, manual annotation of individual granules would provide data also on the granule size, but it is an even more time-consuming method that would

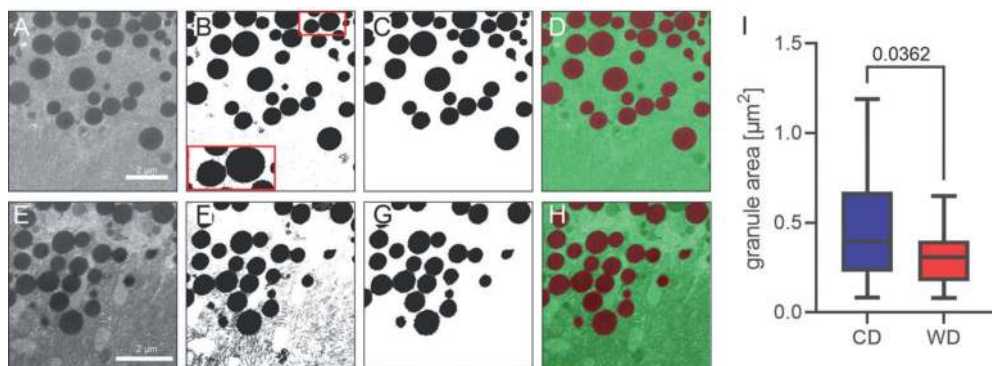


**Figure 7.** Quantitative analysis of the surface area of zymogen granules. Representative TEM images from CD (A) and WD (E) mice. Image thresholding and watershed separation produce a binary mask (B and F), zymogen granules in black, inset depicts exemplary partitioning of two touching granules). Individual granules are determined using particle analysis on the segmented images (C and G). Panels D and H depict an overlay of the granules on the grayscale TEM image (vesicles in red). Quantification of the granule cross-section area shown in the panel I for a given cell from the CD and the WD mouse. Data were pooled from the following number of ROIs from the CD/WD image: 35/27. Data were analyzed using the Mann–Whitney U test, *p* values are indicated on graphs.

effectively hamper analysis or limit it to a few cells only. To at least partially automate the quantification, we took advantage of the fact that zymogen granules have typical properties: (i) granules are spherical structures, and (ii) they appear electron-dense (i.e. dark) on TEM images (Figure 7A and E).

The following brief instructions describe a useful procedure to partition the granules on a TEM image:

1. Image thresholding and separation: Since granules provide good contrast, thresholding the TEM image produces a rough binary mask of granules. Inherently, the thresholding procedure detects two or more granules in close proximity as uniform structures. We can reliably separate the touching granules using the watershed separation method [100]. This method interprets the input image as a topographical surface that is flooded with water, placing water sources in the local topographical minima, and placing dams where water from different sources meets. These dams constitute the watershed (i.e., a border between touching granules, Figure 7B inset). The method works best for smooth convex objects that do not overlap too much, and it efficiently separates granules after the initial thresholding (Figure 7B and E).
2. Particle analysis: Employ particle analysis to remove unwanted small objects in the cytosol that were detected with the thresholding. Limiting the minimal object size effectively removes the background noise (Figure 7C and G).
3. Quantification of the zymogen granules: The resulting binary mask detects individual granules (see the overlay in the Figure 7D and H). The segmentation data generally allow for a straightforward counting of granules, assessing the cumulative granule area (case the entire cell is imaged, example data not shown), and granule size. The latter decreased by 22% in the analyzed acinar cell from a WD treated mouse (Figure 7I).

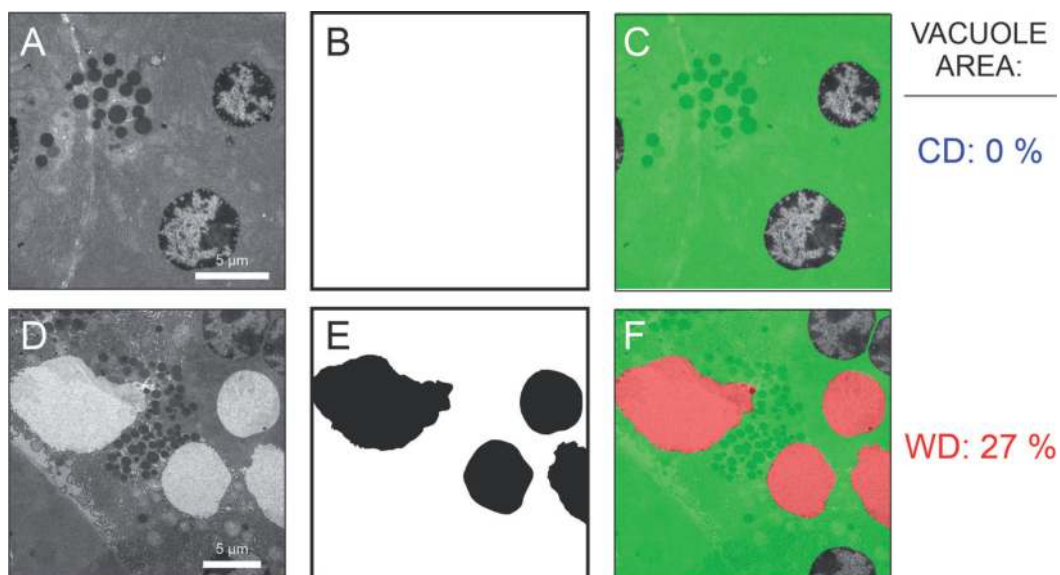


**Figure 8.** Quantitative analysis of the vacuoles. Representative TEM images from CD (A) and WD (E) mice. Manual annotation of vacuoles resulted in a binary mask (B and E), vacuoles in black; please note that no vacuoles were present in A. Panels C and D depict an overlay of the vacuole binary mask on the grayscale TEM image (vacuoles in red, cytoplasm in green). Percentages of vacuole cross-section areas are shown on the right for the CD (blue) and the WD (red) mouse.

#### 5.3.2.4 Analysis of vacuoles

Cytoplasmic vacuolization is an ultrastructural change associated with pathological alterations in pancreatic cells [101]. The vacuoles appear electron-lucent (i.e., bright) and inhomogeneous on TEM images, very similar to other structures, and this does not allow the use of image thresholding as a technique to effectively detect vacuoles. Since the number of vacuoles per cell is limited, manual annotation of the structures is feasible.

1. Manual detection of the vacuoles: Use Fiji/ImageJ in combination with the built-in ROI manager to outline the vacuoles, which results in a binary mask of the visible structures on the image (**Figure 8B** demonstrating an empty mask, since no vacuoles were visible on the image, and **8E** shows several vacuoles that were seen within a cell). Overlaying the structures can serve as visual feedback for quality assessment (**Figure 8C** and **F**).

Quantification of the vacuoles: Use data from the above step to measure the relative area covered by the vacuoles by dividing the cumulative vacuole area by the visible cytoplasm surface. Using this approach, we demonstrated that vacuoles are abundant in the acinar cell of WD treated mice (27% vs. 0% in WD vs. CD mice, **Figure 8** right).

## 6. Conclusions

There are only a handful of studies on pancreatic exocrine and endocrine ultrastructure in mice under diabetogenic conditions. One of the reasons for this relative underrepresentation of such a translationally relevant topic in the literature

may be the rather complex study design typically accompanying work with genetic or dietary mouse models and electron microscopy. An even more important reason may often be a lack of a toolbox to easily, objectively, and reproducibly analyze ultrastructural changes in exocrine and endocrine cells in a quantitative manner. In this chapter, we tried to specifically address this problem by providing the readers with a robust step-by-step approach and detailed instructions on how to quantify changes in the ultrastructure of mitochondria, rough endoplasmic reticulum, and secretory vesicles, as well as the presence of vacuoles, by means of shape descriptors, thresholding, manual selection, and machine-learning supported image segmentation, followed by different quantification steps employed in the open-source Fiji software. With some field-specific modifications, our analyses shall also be useful for many other life scientists.

## **Acknowledgements**

We would like to express our gratitude to colleagues at the Institute of Physiology for their support and to Prof. Gerd Leitinger (Medical University Graz) for critical reading of the manuscript.

## **Funding**

This research was funded by the SLOVENIAN RESEARCH AGENCY, grant number P3-0396, I0-0029, N3-0133, and N3-0170.

## **Author details**

Maša Skelin Klemen<sup>1\*</sup>, Jurij Dolensšek<sup>1,2</sup>, Ismael Valladolid-Acebes<sup>3</sup>, Andraž Stožer<sup>1</sup>  
and Saška Lipovšek<sup>2,4,5,6</sup>

1 Faculty of Medicine, Institute of Physiology, University of Maribor, Maribor, Slovenia

2 Faculty of Natural Sciences and Mathematics, Department of Biology, University of Maribor, Maribor, Slovenia

3 The Rolf Luft Research Center for Diabetes and Endocrinology, Karolinska Institutet, Stockholm, Sweden

4 Faculty of Medicine, University of Maribor, Maribor, Slovenia


5 Faculty of Chemistry and Chemical Engineering, University of Maribor, Maribor, Slovenia

6 Division of Cell Biology, Histology and Embryology, Gottfried Schatz Research Center for Cell Signaling, Metabolism and Aging, Medical University of Graz, Graz, Austria

\*Address all correspondence to: masa.skelin@um.si

## **IntechOpen**

---

© 2022 The Author(s). Licensee IntechOpen. This chapter is distributed under the terms of the Creative Commons Attribution License (<http://creativecommons.org/licenses/by/3.0>), which permits unrestricted use, distribution, and reproduction in any medium, provided the original work is properly cited. 



## References

- [1] IDFIDF Diabetes Atlas. International Diabetes Federation. 2021
- [2] Pørksen N. The in vivo regulation of pulsatile insulin secretion. *Diabetologia*. 2002;**45**(1):3-20
- [3] Simon C, Brandenberger G. Ultradian oscillations of insulin secretion in humans. *Diabetes*. 2002;**51**(suppl\_1):S258-S261
- [4] Simon C. Ultradian pulsatility of plasma glucose and insulin secretion rate: circadian and sleep modulation. *Hormone Research in Paediatrics*. 1998;**49**(3-4):185-190
- [5] Stozer A, Hojs R, Dolensek J. Beta cell functional adaptation and dysfunction in insulin resistance and the role of chronic kidney disease. *Nephron*. 2019;**143**(1):33-37
- [6] Lu H et al. Molecular and metabolic evidence for mitochondrial defects associated with beta-cell dysfunction in a mouse model of type 2 diabetes. *Diabetes*. 2010;**59**(2):448-459
- [7] Irls E et al. Enhanced glucose-induced intracellular signaling promotes insulin hypersecretion: Pancreatic beta-cell functional adaptations in a model of genetic obesity and prediabetes. *Molecular and Cellular Endocrinology*. 2015;**404**:46-55
- [8] Gonzalez A et al. Insulin hypersecretion in islets from diet-induced hyperinsulinemic obese female mice is associated with several functional adaptations in individual beta-cells. *Endocrinology*. 2013;**154**(10):3515-3524
- [9] Corezola do Amaral ME et al. Caloric restriction recovers impaired  $\beta$ -cell- $\beta$ -cell gap junction coupling, calcium oscillation coordination, and insulin secretion in prediabetic mice. *American Journal of Physiology-Endocrinology and Metabolism*. 2020;**319**(4):E709-E720
- [10] Rajab BS et al. Differential remodelling of mitochondrial subpopulations and mitochondrial dysfunction are a feature of early stage diabetes. *Scientific Reports*. 2022;**12**(1):978
- [11] Arrojo EDR, Roy B, MacDonald PE. Molecular and functional profiling of human islets: From heterogeneity to human phenotypes. *Diabetologia*. 2020;**63**(10):2095-2101
- [12] Arrojo EDR. Probing beta-cell biology in space and time. *Diabetes*. 2021;**70**(10):2163-2173
- [13] Titova AA et al. Early ultra- and microstructural alterations in rat pancreas in alloxan-induced diabetes mellitus. *Ultrastructural Pathology*. 2020;**44**(1):61-70
- [14] Lacy PE. Electron microscopic identification of different cell types in the islets of Langerhans of the Guinea pig, rat, rabbit and dog. *The Anatomical Record*. 1957;**128**(2):255-267
- [15] Palade GE. The endoplasmic reticulum. *The Journal of Biophysical and Biochemical Cytology*. 1956;**2**(Suppl. 4):85-98
- [16] Danielsson A et al. The human pancreas proteome defined by transcriptomics and antibody-based profiling. *PLoS One*. 2014;**9**(12):e115421
- [17] Bockman DE. Anatomy of the pancreas. In: Go VLW, editor. *The Pancreas: Biology, Pathobiology, and Disease*. Norris, MT: Raven Press; 1993. pp. 1-8

- [18] In't Veld P, Marichal M. Microscopic anatomy of the human islet of langerhans. In: Islam MS, editor. *The Islets of Langerhans*. Netherlands, Dordrecht: Springer; 2010. pp. 1-19
- [19] Liu XY et al. Pancreas transplantation in the mouse. *Hepatobiliary & Pancreatic Diseases International*. 2010;**9**(3):254-258
- [20] Yaginuma N et al. The microvasculature of the human pancreas and its relation to Langerhans islets and lobules. *Pathology, Research and Practice*. 1986;**181**(1):77-84
- [21] Motta PM et al. Histology of the exocrine pancreas. *Microscopy Research and Technique*. 1997;**37**(5-6):384-398
- [22] Saito K, Iwama N, Takahashi T. Morphometrical analysis on topographical difference in size distribution, number and volume of islets in the human pancreas. *The Tohoku Journal of Experimental Medicine*. 1978;**124**(2):177-186
- [23] Rahier J, Wallon J, Henquin JC. Cell populations in the endocrine pancreas of human neonates and infants. *Diabetologia*. 1981;**20**(5):540-546
- [24] Steiner DJ et al. Pancreatic islet plasticity: Interspecies comparison of islet architecture and composition. *Islets*. 2010;**2**(3):135-145
- [25] Cabrera O et al. The unique cytoarchitecture of human pancreatic islets has implications for islet cell function. *Proceedings of the National Academy of Sciences of the United States of America*. 2006;**103**(7):2334-2339
- [26] Arrojo e Drigo R et al. New insights into the architecture of the islet of Langerhans: A focused cross-species assessment. *Diabetologia*. 2015;**58**(10):2218-2228
- [27] Dolensek J, Rupnik MS, Stozer A. Structural similarities and differences between the human and the mouse pancreas. *Islets*. 2015;**7**(1):e1024405
- [28] Skelin Klemen M et al. The triggering pathway to insulin secretion: Functional similarities and differences between the human and the mouse  $\beta$  cells and their translational relevance. *Islets*. 2017;**9**(6):109-139
- [29] Dolensšek J. *Pancreas Physiology*. London: IntechOpen; 2017
- [30] Hegyi P et al. Pancreatic ductal bicarbonate secretion: Challenge of the acinar acid load. *Frontiers in Physiology*. 2011;**2**:36
- [31] Petersen OH. Physiology of acinar cell secretion. *The Pancreas*. 2008;**26**:69-77
- [32] Argent BE et al. Chapter 51 - Cell Physiology of Pancreatic Ducts, in *Physiology of the Gastrointestinal Tract (Fifth Edition)*, L.R. Johnson, et al., Editors. Boston: Academic Press; 2012. pp. 1399-1423
- [33] Tokarz VL, MacDonald PE, Klip A. The cell biology of systemic insulin function. *The Journal of Cell Biology*. 2018;**217**(7):2273-2289
- [34] Czech MP. Insulin action and resistance in obesity and type 2 diabetes. *Nature Medicine*. 2017;**23**(7):804-814
- [35] Lewis GF et al. Direct and indirect control of hepatic glucose production by insulin. *Cell Metabolism*. 2021;**33**(4):709-720
- [36] Jiang G, Zhang BB. Glucagon and regulation of glucose metabolism. *American Journal of Physiology. Endocrinology and Metabolism*. 2003;**284**(4):E671-E678

- [37] Ramnanan CJ et al. Physiologic action of glucagon on liver glucose metabolism. *Diabetes, Obesity and Metabolism*;13:118-125
- [38] Himsworth HP. Insulin deficiency and insulin inefficiency. *British Medical Journal*;1(4139):719
- [39] Di Ciaula A, Portincasa P. Fat, epigenome and pancreatic diseases. Interplay and common pathways from a toxic and obesogenic environment. *European Journal of Internal Medicine*. 2014;25(10):865-873
- [40] OECD. *The Heavy Burden of Obesity*. Paris, France: OECD; 2019
- [41] Gastaldelli A et al. Relationship between hepatic/visceral fat and hepatic insulin resistance in nondiabetic and type 2 diabetic subjects. *Gastroenterology*. 2007;133(2):496-506
- [42] Goossens GH. The role of adipose tissue dysfunction in the pathogenesis of obesity-related insulin resistance. *Physiology & Behavior*. 2008;94(2):206-218
- [43] Despres JP, Lemieux I. Abdominal obesity and metabolic syndrome. *Nature*. 2006;444(7121):881-887
- [44] Della Corte C et al. Nonalcoholic fatty pancreas disease and nonalcoholic fatty liver disease: More than ectopic fat. *Clinical Endocrinology*. 2015;83(5):656-662
- [45] Petersen KF et al. Reversal of nonalcoholic hepatic steatosis, hepatic insulin resistance, and hyperglycemia by moderate weight reduction in patients with type 2 diabetes. *Diabetes*. 2005;54(3):603-608
- [46] Taylor R et al. Remission of human type 2 diabetes requires decrease in liver and pancreas fat content but is dependent upon capacity for  $\beta$  cell recovery. *Cell Metabolism*. 2018;28(4):547-556
- [47] Acharya C, Navina S, Singh VP. Role of pancreatic fat in the outcomes of pancreatitis. *Pancreatology*. 2014;14(5):403-408
- [48] Navina S et al. Lipotoxicity causes multisystem organ failure and exacerbates acute pancreatitis in obesity. *Science Translational Medicine*. 2011;3(107):107ra110
- [49] Keun Young S et al. Influence of obesity on the severity and clinical outcome of acute pancreatitis. *Gut and Liver*. 2011;5(3):335-339
- [50] Alempijevic T et al. Non-alcoholic fatty pancreas disease. *Postgraduate Medical Journal*. 2017;93(1098):226-230
- [51] Mathur A et al. Nonalcoholic fatty pancreas disease. *HPB*. 2007;9(4):312-318
- [52] Schaefer JH. The normal weight of the pancreas in the adult human being: A biometric study. *The Anatomical Record*. 1926;32(2):119-132
- [53] Ogilvie RF. The islands of langerhans in 19 cases of obesity. *The Journal of Pathology and Bacteriology*. 1933;37(3):473-481
- [54] Taylor R. Remission of type 2 diabetes by weight loss in a non-white population. *The Lancet. Diabetes & Endocrinology*. 2020;8(6):458-459
- [55] Riddle MA-O et al. Consensus report: definition and interpretation of remission in type 2 diabetes. *The Journal of Clinical Endocrinology & Metabolism*;107(1):1-9. DOI: 10.2337/dci21-0034
- [56] Petrov MS, Taylor R. Intra-pancreatic fat deposition: bringing hidden fat to the fore. *Nature Reviews Gastroenterology & Hepatology*. 2021;19:1-16

- [57] Taylor R, Holman RR. Normal weight individuals who develop type 2 diabetes: The personal fat threshold. *Clinical Science*. 2015;**128**(7):405-410
- [58] Cerasi E, Ktorza A. [anatomical and functional plasticity of pancreatic beta-cells and type 2 diabetes]. *Medical Science (Paris)*. 2007;**23**(10):885-894
- [59] Weiss R et al. Beta-cell function across the spectrum of glucose tolerance in obese youth. *Diabetes*. 2005;**54**(6):1735-1743
- [60] White MG, Shaw JA, Taylor RA-O. Type 2 diabetes: the pathologic basis of reversible  $\beta$ -cell dysfunction. *Diabetes Care*. 2016;**39**(11):2080-2088
- [61] Paschen M et al. Diet-induced  $\beta$ -cell insulin resistance results in reversible loss of functional  $\beta$ -cell mass. *The FASEB Journal*. 2019;**33**(1):204-218
- [62] Saito K, Fau-Takahashi T, et al. Islet morphometry in the diabetic pancreas of man. *The Tohoku Journal of Experimental Medicine*. 1978;**125**(2):185-197
- [63] Butler AE et al. Beta-cell deficit in obese type 2 diabetes, a minor role of beta-cell dedifferentiation and degranulation. *The Journal of Clinical Endocrinology and Metabolism*. 2016;**101**(2):523-532
- [64] Marchetti P et al. The endoplasmic reticulum in pancreatic beta cells of type 2 diabetes patients. *Diabetologia*. 2007;**50**(12):2486-2494
- [65] Accili D et al. When beta-cells fail: Lessons from dedifferentiation. *Diabetes, Obesity & Metabolism*. 2016;**18**(Suppl. 1): 117-122
- [66] Hunter CS, Stein RW. Evidence for loss in identity, De-differentiation, and trans-differentiation of islet beta-cells in type 2 diabetes. *Frontiers in Genetics*. 2017;**8**:35
- [67] Talchai C et al. Pancreatic beta cell dedifferentiation as a mechanism of diabetic beta cell failure. *Cell*. 2012;**150**(6):1223-1234
- [68] Cinti F et al. Evidence of beta-cell dedifferentiation in human type 2 diabetes. *The Journal of Clinical Endocrinology and Metabolism*. 2016;**101**(3):1044-1054
- [69] Ajuolabady A et al. ER stress in obesity pathogenesis and management. *Trends in Pharmacological Sciences*. 2022;**43**(2):97-109
- [70] Almanza A et al. Endoplasmic reticulum stress signalling – From basic mechanisms to clinical applications. *The FEBS Journal*. 2019;**286**(2):241-278
- [71] Ariyasu D, Yoshida H, Hasegawa Y. Endoplasmic reticulum (ER) stress and endocrine disorders. *International Journal of Molecular Sciences*. 2017;**18**(2)
- [72] Korc M et al. Pancreatic islet-acinar cell interaction: Amylase messenger RNA levels are determined by insulin. *Science*. 1981;**213**(4505):351-353
- [73] Williams JA, Goldfine ID. The insulin-pancreatic acinar axis. *Diabetes*. 1985;**34**(10):980-986
- [74] Wiederkehr A, Wollheim CB. Minireview: Implication of mitochondria in insulin secretion and action. *Endocrinology*. 2006;**147**(6):2643-2649
- [75] Maassen JA, Janssen GM, Hart LM. Molecular mechanisms of mitochondrial diabetes (MIDD). *Annals of Medicine*. 2005;**37**(3):213-221
- [76] Ma Z et al. Diabetes reduces beta-cell mitochondria and induces distinct

- morphological abnormalities, which are reproducible by high glucose in vitro with attendant dysfunction. *Islets*. 2012;**4**(3):233-242
- [77] Anello M et al. Functional and morphological alterations of mitochondria in pancreatic beta cells from type 2 diabetic patients. *Diabetologia*. 2005;**48**(2):282-289
- [78] Masini M et al. Ultrastructural alterations of pancreatic beta cells in human diabetes mellitus. *Diabetes/ Metabolism Research and Reviews*. 2017;**33**(6):e2894
- [79] Folli F et al. Pancreatic islet of Langerhans' cytoarchitecture and ultrastructure in normal glucose tolerance and in type 2 diabetes mellitus. *Diabetes, Obesity & Metabolism*. 2018;**20**(Suppl. 2):137-144
- [80] Jung HS, Lee MS. Role of autophagy in diabetes and mitochondria. *Annals of the New York Academy of Sciences*. 2010;**1201**:79-83
- [81] Jung HS, Lee MS. Macroautophagy in homeostasis of pancreatic beta-cell. *Autophagy*. 2009;**5**(2):241-243
- [82] Masini M et al. Autophagy in human type 2 diabetes pancreatic beta cells. *Diabetologia*. 2009;**52**(6):1083-1086
- [83] Dimmer KS, Scorrano L. (De) constructing mitochondria: What for? *Physiology (Bethesda)*. 2006;**21**:233-241
- [84] Joost H-G, Al-Hasani H, Schurmann A. Animal models in diabetes research. In: *Methods in Molecular Biology*. xi ed. New York: Humana Press; 2012. p. 325
- [85] Fellmann L et al. Murine models for pharmacological studies of the metabolic syndrome. *Pharmacology & Therapeutics*. 2013;**137**(3):331-340
- [86] Gill-Randall RJ et al. Is human type 2 diabetes maternally inherited? Insights from an animal model. *Diabetic Medicine*. 2004;**21**(7):759-762
- [87] Kaplan JR, Wagner JD. Type 2 diabetes - an introduction to the development and use of animal models. *ILAR Journal*. 2006;**47**(3):181-185
- [88] King AJF. The use of animal models in diabetes research. *British Journal of Pharmacology*. 2012;**166**(3):877-894
- [89] Winzell MS, Ahrén B. The high-fat diet-fed mouse: A model for studying mechanisms and treatment of impaired glucose tolerance and type 2 diabetes. *Diabetes*. 2004;**53**(suppl 3):S215-S219
- [90] Stožer A et al. Confocal laser scanning microscopy of calcium dynamics in acute mouse pancreatic tissue slices. *JoVE*. 2021;**170**:e62293
- [91] Stožer A, Dolenšek J, Rupnik MS. Glucose-stimulated calcium dynamics in islets of Langerhans in acute mouse pancreas tissue slices. *PLoS One*. 2013;**8**(1):e54638
- [92] Speier S, Rupnik M. A novel approach to in situ characterization of pancreatic  $\beta$ -cells. *Pflügers Archiv European Journal of Physiology*. 2003;**446**(5):553-558
- [93] Brereton MF et al. Alpha-, delta- and PP-cells: Are they the architectural cornerstones of islet structure and co-ordination? *Journal of Histochemistry & Cytochemistry*. 2015;**63**(8):575-591
- [94] Pfeifer CR et al. Quantitative analysis of mouse pancreatic islet architecture by serial block-face SEM. *Journal of Structural Biology*. 2015;**189**(1):44-52
- [95] Leiter EH, Fau-Gapp DA, et al. Ultrastructural and morphometric studies

of delta cells in pancreatic islets from C57BL/Ks diabetes mice. *Diabetologia*. 1979;17(5):297-309

[96] Lipovšek S et al. Rab3a ablation related changes in morphology of secretory vesicles in major endocrine pancreatic cells, pituitary melanotroph cells and adrenal gland chromaffin cells in mice. *General and Comparative Endocrinology*. 2013;185:67-79

[97] Zeidler A et al. Assessment of pancreatic islet-cell population in the hyperglycemic athymic nude mouse: immunohistochemical, ultrastructural, and hormonal studies. *Pancreas*. 1989;4(2):153-160

[98] Schindelin J et al. Fiji: An open-source platform for biological-image analysis. *Nature Methods*. 2012;9(7):676-682

[99] Arganda-Carreras I et al. Trainable Weka segmentation: A machine learning tool for microscopy pixel classification. *Bioinformatics*. 2017;33(15):2424-2426

[100] Legland D, Arganda-Carreras I, Andrey P. MorphoLibJ: Integrated library and plugins for mathematical morphology with ImageJ. *Bioinformatics*. 2016;32(22):3532-3534

[101] Abdul-Hamid M, Moustafa N. Protective effect of curcumin on histopathology and ultrastructure of pancreas in the alloxan treated rats for induction of diabetes. *The Journal of Basic & Applied Zoology*. 2013;66(4):169-179